Journal of Photonics for Energy

PhotonicsforEnergy.SPIEDigitalLibrary.org

Inexpensive organic dyes-sensitized zinc oxide nanoparticles photoanode for solar cells devices

Samy Shaat
Hamdiya Zayed
Hussam Musleh
Nabil Shurrab
Ahmed Issa
Jihad Asad
Naji Al Dahoudi

SPIE.

Samy Shaat, Hamdiya Zayed, Hussam Musleh, Nabil Shurrab, Ahmed Issa, Jihad Asad, Naji Al Dahoudi, "Inexpensive organic dyes-sensitized zinc oxide nanoparticles photoanode for solar cells devices," *J. Photon. Energy* **7**(2), 025504 (2017), doi: 10.1117/1.JPE.7.025504.

Inexpensive organic dyes-sensitized zinc oxide nanoparticles photoanode for solar cells devices

Samy Shaat,[a,*] Hamdiya Zayed,[b] Hussam Musleh,[b,c] Nabil Shurrab,[d] Ahmed Issa,[e] Jihad Asad,[c] and Naji Al Dahoudi[c]

[a]Islamic University of Gaza, Faculty of Science, Department of Physics, Gaza, Palestine
[b]Ain Shams University, Women's College for Art, Science, and Education, Department of Physics, Cairo, Egypt
[c]Al Azhar University-Gaza, Faculty of Science, Department of Physics, Gaza, Palestine
[d]Al Azhar University-Gaza, Faculty of Science, Department of Chemistry, Gaza, Palestine
[e]Al Azhar University-Gaza, Faculty of Engineering and IT, Department of Engineering, Gaza, Palestine

Abstract. Zinc oxide nanoparticles (ZnO NPs) were synthesized using a hydrothermal route. The prepared ZnO NPs were characterized by x-ray diffraction (XRD), high-resolution transmission electron microscopy (HR-TEM), UV–vis spectroscopy, and photoluminescence (PL) spectroscopy. The XRD patterns confirmed the standard hexagonal wurtzite structure of ZnO NPs, and the calculated value of the average particle size was 23.34 nm. HR-TEM micrographs of ZnO NPs showed semispherical particle morphologies and their sizes lie between 10 and 40 nm. The estimated average size distribution of ZnO NPs was 21.35 ± 6.01 nm. UV–vis spectrum of ZnO NPs revealed the highest absorption band at 360.5 nm, and the E_g was 3.70 ± 0.01 eV. The PL spectrum emission was deconvoluted by eight peaks into two regions [near-ultraviolet (NUV) and visible that caused from the defects]. Two groups of dye-sensitized solar cells (DSSCs) thin film devices based on ZnO NPs were sensitized in different concentration solutions of 0.1, 0.32, and 0.5 mM of eosin B (EB) and eosin Y (EY) dyes. The sensitized DSSCs device with 0.32-mM dye of EY displayed higher efficiency and its performance parameters are much better among all other fabricated DSSCs devices. The short current density (J_{sc}) increased from 1.59 to 4.97 mA/cm^2 and the V_{oc} enhanced from 0.36 to 0.46 V. The conversion efficiency from light to electricity showed a significant improvement from 0.29% to 0.94%. The transient open circuit photovoltage decay (TOCPVD) was measured to estimate the apparent electron lifetime or response time (τ_n) or the electron recombination rate (k_{rec}), using the double exponential function for first time to fit the experiment data of TOCPVD. The results revealed that the EY dye can be used as an efficient and an inexpensive dye for DSSCs. [DOI: 10.1117/1.JPE.7.025504]

Keywords: clean renewable energy; eosin DSSCs; defects; photoluminescence; transient open circuit photovoltage decay; lifetime; traps; electron recombination; solar cells.

Paper 17027 received Mar. 14, 2017; accepted for publication May 16, 2017; published online Jun. 15, 2017.

1 Introduction

The worldwide energy shortage and crisis drove humankind into a quest of alternative energy solutions. Scientists, economists, and politicians face tremendous challenges to find out the alternative clean renewable energy (CRE) resources.[1] Among these, solar energy (SE) is one of the most active research areas for many researchers. It is worth mentioning that, the hourly SE flux arriving to earth is as much as the global power consumption. Thus, the sun is considered as an abundant source of CRE. Therefore, investigators and workers have been paying more

*Address all correspondence to: Samy Shaat, E-mail: sshaat@gmail.com

1947-7988/2017/$25.00 © 2017 SPIE

attention to convert the SE radiation to electricity by fabricating the photovoltaic solar cells (PVSCs). More than one generation of PVSCs were reported in the literature such as the silicon-based solar cells (SBSCs) and dye-sensitized solar cells (DSSCs) that are considered as a new class of photoelectrochemical cells based on nanoscale porous metal oxide semiconductors. The high cost of SBSCs is the main factor that still limits the implementation of solar electricity on wide scales.[2] On one hand, DSSCs[3] present a new model of PVSCs, which is very different from the SBSCs, as they do not rely on a traditional p-n heterojunction to separate photogenerated charge carriers. They were introduced as the third generation of PVSCs after the SBSCs and the thin film solar cells.[4] DSSCs are cost effective and easy to fabricate. Nevertheless, they are still widely investigated to improve their efficiency. The DSSCs are a mimic of the photosynthesis and the physical separation between photon absorption and charge percolation process. Herein, the SE radiation is absorbed by the dye molecules that are attached to the surface of a photoanode layer synthesized from semiconductor nanoparticles. As a result, the free charges are injected into the photoanode layer while the dye molecules are regenerated via reduction by a redox shuttle electrolyte. The oxidized electrolyte is diffused to a counter electrode to complete the circuit. The recombination of the injected electron with the oxidized dye before it is regenerated, or the redox shuttle, can intercept an electron from the photoanode before it is collected. This causes a drop on the total performance of the conversion process. It is clear that the photogeneration, separation, and recombination take place nearly exclusively at the high-surface area with different interfaces, and thus the properties of these interfaces are of critical importance to the conversion efficiency of the DSSCs devices. In the last decade, different n-type metal oxide semiconductors were used as a photoanode in DSSCs from a principle point of view such as ZnO, TiO_2, SnO_2, In_2O_3, and Nb_2O_5. Currently, common photoanode materials that are used as a thin film layer on transparent conducting oxide in DSSCs are TiO_2 and ZnO nanoparticles (ZnO NPs).[5] Among these materials, ZnO has a slightly higher conduction band level compared to those of TiO_2 and a superior electron mobility, which, in turn, allows for the generation of higher open-circuit voltage and facile electron transport. Additionally, ZnO nanostructures with large surface areas can be realized.[6] Dye-sensitized TiO_2 and ZnO DSSCs have attracted considerable attention in both science and technology.[7] In addition, versatile ZnO is having a large exciton binding energy of ~60 meV at room temperature,[8] and a wide bandgap (3.37 eV) with very high electron mobility (155 $cm^2\ V^{-1}\ s^{-1}$).[9] The properties of ZnO including their piezoelectricity, electrical conductivity, biocompatibility, and UV-visible luminescence have led to numerous applications in various fields including piezoelectric devices, biolabeling, light-emitting diodes, and short-wavelength nanolasers.[8] The popularity of such materials is due to their large surface area and chemical affinity for adsorption of molecules of dye as well as their suitable energy band gap for charge transfer from dye to electrolytes.[10,11] The structure and morphology of the photoelectrode play a vital role in developing such materials.[12,13] The improvement of the conversion efficiency can be attributed to the larger surface area, which is a goal of most researchers in the field. However, a sufficient absorption of the solar spectrum is the start for any power conversion. Therefore, the nature of the adsorbed anchored dyes on the surface of the semiconductor is a crucial factor to enhance the performance of such cells.

To date, two kinds of dyes, namely, metal-organic complexes, e.g., ruthenium (Ru) (II) polypyridyl complexes[14–16] and metal-free organic dyes (MFODs),[17–19] have been widely used as sensitizers of DSSCs. There are different factors that make MFODs good candidates for DSSCs devices: (1) inexpensive, because they do not contain noble metals such as Ru; (2) their relatively large absorption coefficient; (3) easy to be recycled; and (4) the ability to control their absorption spectra via molecular design. Although Ru complexes have many disadvantages, there are still some problems to be solved in terms of higher cost, preparation, and purification. In this regard, organic sensitizers are recently considered as the alternative to Ru complexes. Among the organic sensitizers, eosin-Y ($C_{20}H_6Br_4Na_2O_5$) from xanthene series is one of the best sensitizers and much cheaper than the Ru complexes dyes.[9] In addition, the DSSCs based on eosin dyes is more stable than that based on the Ru dyes, where Ru dyes deteriorate the surface of the ZnO NPs. In this work, ZnO NPs were synthesized via a simple method for use as a photoanode for the DSSCs without blocking layer and no double layers. The structural and optical properties of

the synthesized, ZnO NPs were investigated. When compared with other organic dyes, eosin B (EB) and eosin Y (EY) were used as a photosensitizer that are bound to the surface of the ZnO NPs, which are thousand times cheaper than the Ru-based dye, and it is easier to recycle metal-free dye-based cells.[20] The comparison between the two dyes in terms of the assembled DSSCs performance was reported. Our ongoing work is based on the modification of eosin dyes by adding some functional groups to enhance the performance of the harvesting and electron injection of such dyes.

2 Experimental

2.1 *Synthesis of ZnO Nanoparticles*

ZnO NPs were synthesized using the hydrothermal method. Eight-grams of zinc acetate $[Zn(CH_3COO)_2 \cdot 2H_2O]$ was dissolved in 100 ml of pure methanol. After vigorous stirring for 30 min at a temperature of 60°C and sonication for 30 min, a colorless homogeneous solution was obtained. A 5M NaOH was added dropwise into the solution under continuous and vigorous stirring to adjust the pH to be 14. The colorless homogeneous solution changed to milky white slurry colloid. The milky white colloid was stirred for 60 min at a temperature of 60°C. The colloid was transferred to a 100-ml Teflon lined stainless steel autoclave for 3 h at a temperature of 160°C. After that, a white precipitate was carefully collected and then centrifuged at 3500 rpm by washing five times for 90 min with absolute ethanol to remove the debris, the excess salts, and the leftover unreacted materials. Finally, the residual product was left to dry overnight at a temperature of 120°C, and then, crushed into powder form.

2.2 *Fabrication and Assembly of the DSSCs Devices*

The paste of ZnO NPs was prepared by mixing ZnO NPs and polyethylene glycol (PEG 400) with the ratio 1:2 using a mortar and pestle for 10 min. The paste was deposited on fluorine-doped SnO_2-coated glass substrates, using the "doctor blade" technique forming 0.5×0.5 cm^2 layers. The layers were dried at 100°C for 60 min followed by sintering at 450°C for 60 min in air. The thickness of the obtained sintered layers was measured and lies between 12 and 15 μm. The prepared ZnO NPs photoanode films were divided into two groups, I and II. Groups I and II were, separately, immersed in different concentration solutions of 0.1, 0.32, and 0.5 mM of EB ($C_{20}H_8Br_2N_2O_9$) and EY ($C_{20}H_6Br_4Na_2O_5$) dyes to sensitize them. After 24 h, the films were rinsed in ethanol and were air dried at room temperature. A Pt-coated silicon substrate was used as the counterelectrode where the liquid electrolyte was the iodide-based solution, which consists of 0.6M tetra-butylammonium iodide, 0.1M lithium iodide, 0.1M iodine, and 0.5M 4-tert-butylpyridine in acetonitrile.

The photovoltaic DSSCs devices were characterized using a simulated AM 1.5 sunlight illumination with an output power of 100 mW cm^2. To measure the adsorbed dye amount on the films, the dye was desorbed by immersing dye-sensitized films in a 0.1M NaOH solution in water and ethanol (1:1, v/v). An ultraviolet–visible spectrophotometer (UV–vis) was employed to measure the dye concentration of the desorbed-dye solution. The transient open-circuit photovoltage decay (TOCPVD) experiment was conducted by monitoring the subsequent decay of TOCPVD due to turning off the light source after illuminating the DSSCs devices based on 0.32 mM of the EB and EY dyes for few minutes following the technique used by Zaban et al.[21]

2.3 *Measurements and Characterization Techniques*

The structure of the prepared ZnO NPs samples was investigated with a range of wide Bragg's angle ($2\theta = 25$ deg to 75 deg) using Philips Expert, x-ray diffraction (XRD) equipped with Cu-Kα radiation ($\lambda = 1.5418$ Å), employing a scanning rate of 0.02 s^{-1}. High-resolution transmission electron microscopy (HR-TEM) micrographs were obtained using (JEM-2100),

JEOL electron microscope operated using 200 kV. Samples for HR-TEM studies were prepared by placing a drop of nanosuspension on a carbon-coated Cu grid, and the solvent was evaporated at room temperature. A small quantity of prepared ZnO nanopowder was dissolved in ethanol to measure the UV–vis absorption and photoluminescence (PL) emission. The UV–vis absorption measurements were performed using double beam shimadzu UV-1601 PC with a diffraction grating with a self-aligning, energy-optimizing deuterium lamp for ultraviolet region and halogen lamp for the visible region to enhance the accuracy across the UV–vis. All PL emission spectra were measured with spectrofluorimeter model SPF-200 (Biotech Engineering Management Co., UK). PL measurements were conducted at room temperature using 150 W xenon lamp with a high-sensitivity photomultiplier tube, as a detector in the range from 350 to 900 nm and the excitation wavelength was 320 nm.

3 Results and Discussion

3.1 *X-Ray Diffraction Patterns Analysis*

Crystallography structure phase and lattice parameters of the as-synthesized ZnO NPs can be investigated by XRD technique. Figure 1 shows the intense and crystalline XRD patterns of the as-synthesized ZnO NPs, which were recorded at room temperature. All the diffraction peaks are indexed to the standard hexagonal wurtzite structure of ZnO NPs (inorganic crystal structure database number ICSD-52362). The sharpness of the broadened XRD diffraction peaks is an indication of the small size and the good crystallinity of the NPs. In addition, no peak corresponding to any impurity could be seen and this confirms the formation of single phase of ZnO NPs. The preferred orientation corresponding to the plane (101), which overwhelms the other peaks, is the most prominent peak, which agrees with the results of Kumar et al.[22] Based on the Scherrer equation, the estimated average crystallite size of the ZnO NPs has been obtained from the highest diffraction peak along the (101) plane. The calculated value of the average crystallite size is 23.34 nm.

3.2 *HRTEM Analysis of ZnO NPs*

HR-TEM bright-field photomicrographs were used to conclude the actual shape and size distribution of the as-synthesized ZnO NPs. As shown in Fig. 2(a), the HR-TEM micrograph suggests that ZnO NPs are, well, crystallized with an intermediate or poor agglomeration.

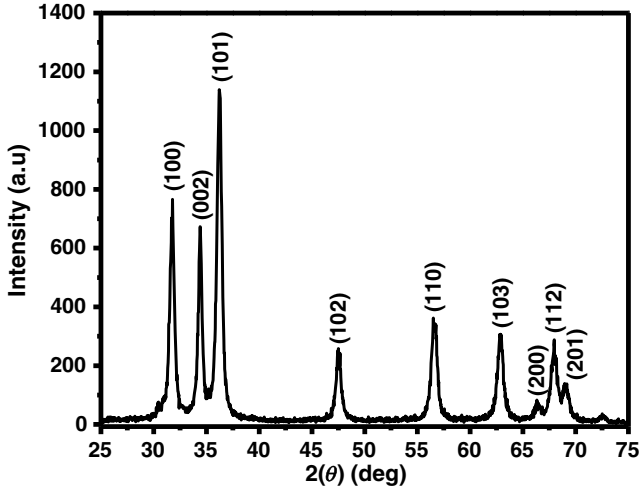

Fig. 1 XRD patterns of the as-synthesized ZnO NPs.

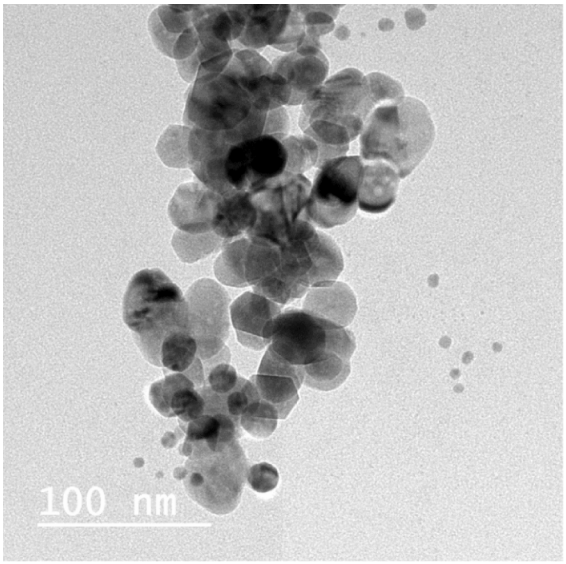

(a)

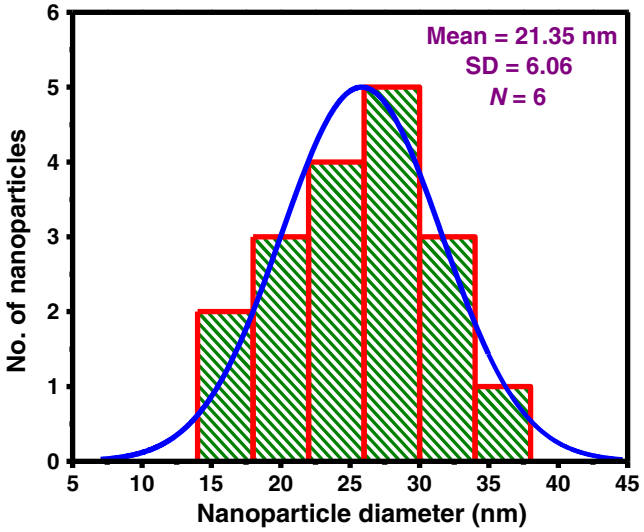

(b)

Fig. 2 (a) HR-TEM image of ZnO NPs and (b) particle size histogram with a solid (blue) line represents the size distribution fit to a normal function used to determine the distribution mean-size and SD.

Moreover, as presented in Fig. 2(a), the HR-TEM image shows the distribution of semi-pherical morphologies of ZnO NPs with a particle size lying between 10 and 40 nm. Ghosh et al.[23] reported the same morphology of ZnO NPs. The quantitative analysis of the size distribution for the ZnO NPs was achieved by plotting the histogram in Fig. 2(b). The size distribution of ZnO NPs is given by mean $\pm$ standard deviation (SD) that can be produced from fitting the histogram using the normal function [solid blue line in Fig. 2(b)]. The estimated average size distribution of ZnO NPs is 21.35 ± 6.01 nm. It is evident that the estimated size distribution of ZnO NPs from HR-TEM images is in good agreement with the average crystallite size that was calculated from the XRD patterns using Scherrer method.

3.3 *UV–Vis Study*

Figure 3 presents a typical optical absorption spectrum of sample as-synthesized ZnO NPs fabricated in this work. It is clear that the sample has a very high absorbance in the UV region and

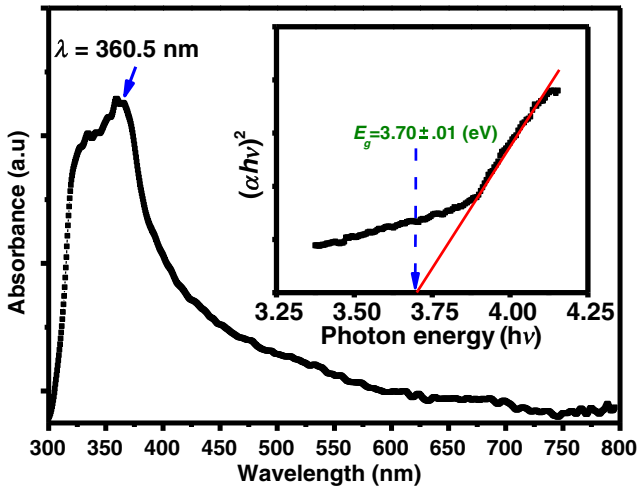

Fig. 3 UV–vs absorption spectrum of ZnO NPs and the inset is $(\alpha h\nu)^2$ versus the photon energy $(h\nu)$.

decreases exponentially with increasing wavelength, which indicates that ZnO NPs have high response in the UV region. Moreover, the highest absorption band can be observed at 360.5 nm, which is attributed to the bandband transition of the ZnO NPs. This exciton absorption peak is observed at 360.5 nm due to ZnO NPs being below the band gap wavelength of bulk ZnO (388 nm) and indicates monodispersing of ZnO NPs as suggested by Brintha et al.[24] The sharp absorbance peak onset at about 360.5 nm is also a strong indication of an almost uniform size of the as-synthesized ZnO NPs. The edge of allowed direct optical bandgap energy (E_g) of ZnO NPs was determined using the Tauc Davis and Mott equation,[25] $(\alpha h\nu)^2 = S(h\nu - E_g)$, where S is constant, α is the absorption coefficient of the material, and $h\nu\,(\text{eV}) = 1239.7/\lambda\,(\text{nm})$ is the photon energy. E_g was estimated by plotting $(\alpha h\nu)^2$ versus $h\nu$ as shown in the inset of Fig. 3. E_g of ZnO NPs was estimated by extrapolating the linear region to the abscissa, i.e., $(\alpha h\nu)^2 = 0$, yielding $E_g = 3.70 \pm 0.01$ eV. The estimated energy bandgap is agreed well with the obtained result in Ref. 26. This value of E_g indicates that a blueshift occurred in our sample. This can be interpreted as bandgap widening that occurs in semiconductors as demonstrated by Kim et al.[27] This blueshift may be attributed to quantum confinement effects according to Aneesh et al.[28]

3.4 *Photoluminescence Study*

PL technique is considered a good optical method for probing electron transitions between high- and low-energy levels as well as for finding electron densities of states.[29] On one hand, it can be used to detect impurities, defects, traps, and imperfections in materials, as well as to estimate the bandgaps of materials. The PL emission spectrum (PLES) of ZnO NPs typically exhibits a linear emission in the NUV range (originating from exciton mechanism) and in the visible region, which is connected to defects in ZnO NPs.[23] It is well known that the PLES of ZnO nanocrystals in the visible region is due to the defects or interior energy traps (IETs) present within the bandgap, such as vacancies, impurities, imperfections, interstitials, Zn residues, and antisites, mainly, from the various oxygen vacancies,[30,31] which play an important role in various applications such as the performance of the DSSCs. Therefore, it is difficult to identify the IETs that may be produced, simultaneously, during the preparation method.[23] Figure 4 shows the room temperature PLES of the as-synthesized ZnO NPs, which is recorded at excitation wavelength of 320 nm. The PLES is understood by the deconvolution consisting of eight peaks as shown in Fig. 4. The main features of the PLES of ZnO NPs can be decomposed into two regions: NUV and visible. For the PLES of NUV region, the positions of the emission peaks are centered at 349.31 (3.55 eV) and 382.79 nm (3.24 eV). The NUV can be subjected to the near-band edge (NBE) emission due to the radiative recombination of free excitons through an exciton–exciton collision process.[22] The NBE emission from the ZnO nanocrystals strongly indicates the

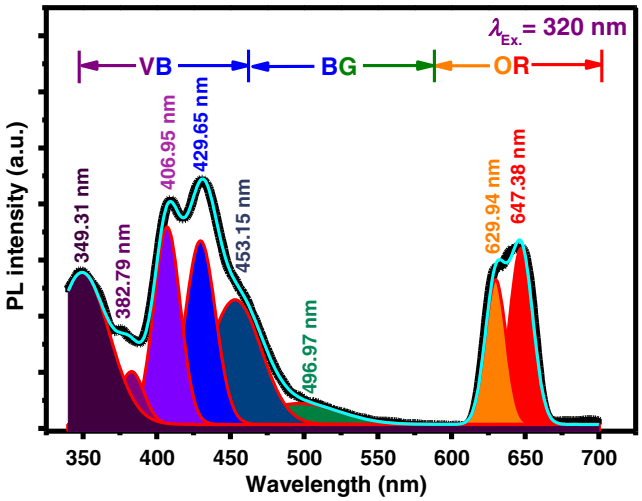

Fig. 4 PLES and deconvoluted peaks of ZnO NPs was excited at 320 nm.

presence of $Zn(OH)_2$.[32] In the visible region, the PLES can be divided into three categories: violet-blue (VB), blue-green (BG), and orange-red (OR). Different types of IETs are presumed to explain the observed emission bands in the visible range. The VB emission can be decomposed into two peaks centered at 406.95 (3.05 eV) and 429.65 nm (2.89 eV). The VB emission peaks are assigned to the transition of electron from the bottom (donor) of conduction band to the energy level of Zn vacancy (V_{Zn}), which infers that the ZnO NPs are n-type semiconductors.[29] For the BG emission, it consists of two peaks centered at 453.15 (2.73 eV) and 496.94 nm (2.49 eV). The BG emission is caused by the transition of electrons from conduction band edge to the IETs complex (V_{ZnO}).[30] The OR emission can be disbanded into two peaks centered at 629.94 (1.37 eV) and 647.37 nm (1.31 eV). Generally, the OR centered at ~600 to 760 nm is attributed to deep IETs interstitial and vacancies of oxygen (O_i and V_o), respectively, in ZnO NPs.[22,31] From our view, when the GB emission diminishes, OR emission at higher wavelength (low energy) will be intense. By comparing our results to other published articles, it is possible to find a blueshift in the peaks positions due to the different kinds of transitions. The increased blueshift in the emission spectrum for ZnO NPs is most likely due to a reduction in the NPs aggregation, which is in agreement with the HR-TEM results in Fig. 2. The reduced aggregation is understood to result in a higher number of interfaces with the NPs. The increased blueshift can also be explained to arise from band bending due to a depletion layer in smaller spherical particles, which is absent in the larger particles with flat faces.[23,30,33,34] The ratio between the areas of the NBE and the IETs emissions is an indicator of the quality of ZnO (i.e. the ratio of the defects in the ZnO). This is very important to determine the usage of the ZnO. For example, in the DSSCs, a high ratio of defects (IETs emissions) is required. As shown in Fig. 4, the area under the IETs emissions was found to be more than the area under the NBE emissions. This indicates that the ratio of defects in ZnO is high.

3.5 *Solar Cell Performance*

The performance of the ZnO NPs photoanode that were sensitized with different concentrations of single EB, and EY dyes were examined. The characteristic $J-V$ curves of different fabricated DSSCs devices with different concentrations of single EB and EY are shown in Figs. 5 and 6, respectively. The calculated values of the photovoltaic performance parameters for all fabricated DSSCs devices are listed in Table 1, in which the sensitized cell with the concentration of 0.32-mM EY dye exhibited the highest efficiency and best performance, which has the following performance parameters: open-circuit voltage $V_{oc} = 0.46$ V, short circuit photocurrent density $J_{sc} = 4.97$ mA cm^2, maximum power $P_m = 2.29$, fill factor FF $= 41.46\%$, and efficiency $\eta = 0.94\%$. The highest P_m was recorded for the signed DSSCs device with 0.32-mM EY dye, whereas the lowest P_m was registered for the marked DSSCs device with 0.5-mM EB

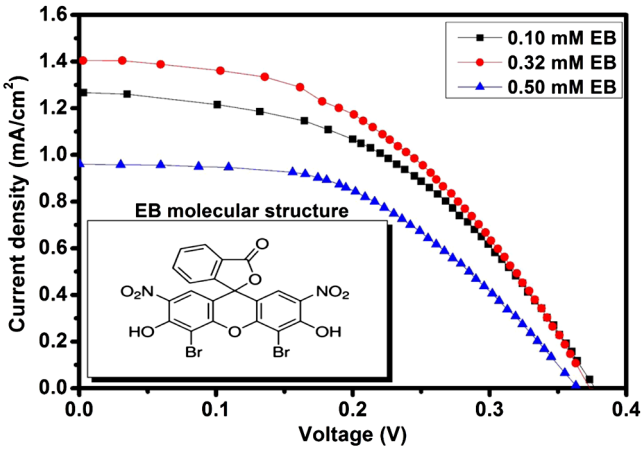

Fig. 5 Characteristic $J-V$ curves for DSSCs made from ZnO NPs photoanode at different concentrations of EB dye, the inset is the EB molecular structure.

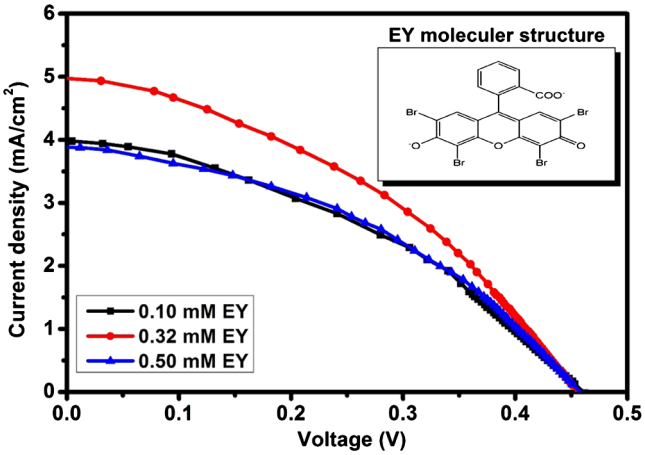

Fig. 6 Characteristic $J-V$ curves for DSSCs made from ZnO NPs photoanode at different concentrations of EY dye, the inset is the EY molecular structure.

Table 1 Photovoltaic performance parameters for DSSCs devices made from ZnO NPs photoanode films for different concentrations of EB and EY dyes.

	J_{sc} (mA/cm^2)		V_{oc} (V)		FF		η (%)	
Dye conc. (mM)	EB	EY	EB	EY	EB	EY	EB	EY
0.1	1.27	3.34	0.37	0.46	46.76	46.31	0.22	0.70
0.32	1.59	4.97	0.36	0.46	49.76	41.46	0.29	0.94
0.5	0.36	3.54	0.35	0.45	49.63	44.96	0.17	0.73

dye. In Table 1, comparison of results for cells fabricated with EB dye to those fabricated with EY dye at a fixed concentration of 0.32 mM is shown. It is evident that cells with EY dye displayed higher efficiency, and their performance parameters are much better among all fabricated DSSCs devices. It was expected that high dye loading may result in poor stability and deterioration of the performance of the ZnO NPs because of the acidic-binding groups that can lead to dissolution of ZnO NPs and precipitation of complexes consisting of the dye and Zn^{2+} ions.[35] The electron injection efficiency can also be influenced by the aggregation of dye molecules on the metal oxide surface, where less aggregated dye anchoring onto the metal oxide should be

desirable for faster electron injection.[36] It is further noticed from this comparison that, the J_{sc} increased from 1.59 to 4.97 mA/cm^2 and the V_{oc} was enhanced from 0.36 to 0.46 V. Ultimately, the results indicated that the conversion efficiency from light to electricity showed a significant improvement from 0.29% to 0.94%.

The lower energy conversion efficiency in the DSSCs devices could be attributed to the lower amount of dye adsorbed in the ZnO NPs film resulting in lower absorption of light, which reduces the injection efficiency of charge carriers into the photoanode. The previous results showed an enhancement of both the J_{sc} and the V_{oc} in the case of the EY dye compared to the case of the EB dye, which may be attributed to the higher dye loading of the EY on the surface of the ZnO NPs. Figure 7 shows the dye uptake of both EB and EY dyes normalized to the same area. The calculated amount of dye adsorbed per unit area is 1.3×10^{-7} mol/cm^2 for the EB sample and 3.9×10^{-7} mol/cm^2 for the EY one. The EY samples exhibit larger absorption compared with the EB one. The significant increasing of the dye loading of EY may explain the high J_{sc} compared with that for EB. It is expected that EY attached very well onto the surface of the ZnO NPs film, which is more negative than EB, whereas the electrostatic attractive forces are stronger than that of EB. The extinction coefficient of EY is 1226, which is much larger than that of EB (549),[37] which mean higher harvesting ability for the photons. The difference in the V_{oc} for both dyes refers to the faster recombination process for the cell based on the EB dye. The generated electrons in DSSCs based on the EB dye can be recombined with triiodide at the ZnO/electrolyte interface faster than those in the case of DSSCs based on EY dye. The differences in the photoinduced current density (J) were generated by the EY dye that is attributed to the upward shift movement of the conduction band edge and conversely for EB dye. The V_{oc} is related to the energy difference between the Fermi level of the metal oxide and the Nernst potential of the redox couple in the electrolyte. The electron injection into the conduction band of metal oxide results in an increase in electron density, raising the Fermi level toward the conduction band edge (band bending). This shift of the Fermi level of metal oxide under irradiation increases the free energy of injected electrons, which is responsible for the generation of the photovoltage in the external circuit.[38] The downward shift of the conduction band edge leads to a lower V_{oc}, which indicates that the photoinduced electron density solely determines the difference between the conduction band edge and the electron quasi-Fermi level under illumination.[39] In addition, in terms of the dye loading and the light scattering, it is widely agreed that the charge-transition kinetics play a significant role in understanding the performance of DSSCs devices such as the conversion efficiency.[40] According to the suggested simple model of the DSSCs by Ref. 41 at short circuit, different charge-transition processes can exist in the DSSCs devices, in which the slower recombination process is preferable. It is well known that the charge presents more than one kind of motion status at different voltage-dependent

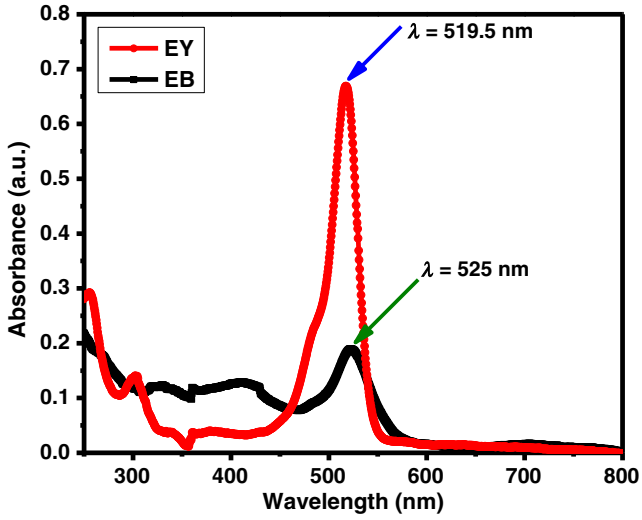

Fig. 7 UV–vis adsorption spectra of EB and EY dyes absorbed by ZnO NPs film.

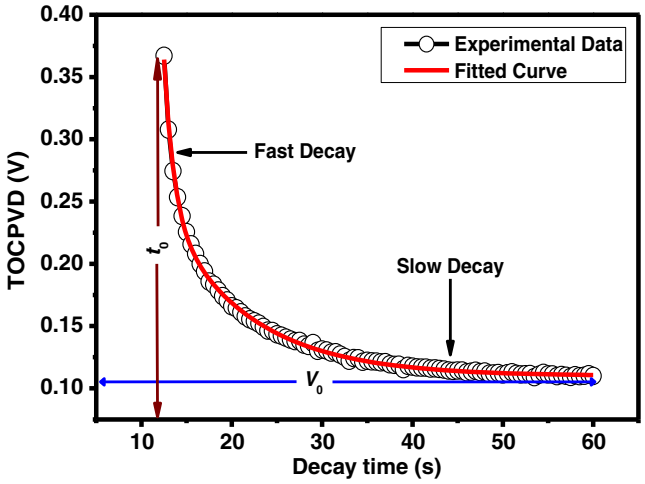

Fig. 8 TOCPVD of DSSCs device based 0.32-mM of EB dye and the red line is the double exponential decay fitted curve.

regions.[40] Among them, the exponential increase region relates to internal trapping of the photoanode material, which reveals the apparent electron lifetime or response time (τ_n) or the electron recombination rate (k_{rec}) in the photoanode material. The TOCPVD measurements were carried out on the fabricated DSSCs devices to obtain the τ_n or k_{rec}. Figures 8 and 9 show TOCPVD experiment for the DSSCs devices, based on the 0.32 mM of EB and EY dyes, which follow a pseudoexponential (semilog) form. Two decayed components are distinguished: fast and slow decays, which may be attributed to their intrinsic material properties.[42] This, also, may be attributed to the different defects of the ZnO NPs that were discussed in the PL results earlier. A double exponential function fits the TOCPVD data as in Eq. (1) to extract the decay parameters

$$V_{\text{OC}} = V_0 + V_1 e^{-(t-t_0)/\tau_1} + V_2 e^{-(t-t_0)/\tau_2}, \tag{1}$$

where V_0 is the offset of the V_{OC}, V_1 and V_2 are the amplitudes of V_{OC} of the two fitting curves, t is the decay time, t_0 is the center of the fitting curve, and τ_1 and τ_2 are the decay time constants (lifetime). The second and third terms on the right-hand side of Eq. (1) describe the fast and slow decays, respectively. Equation (1) indicates that different decay mechanisms are excited during the TOCPVD process. τ_n is an important parameter that renders a better understating of the photovoltaic system. As it was reported in Ref. 21, the τ_n is determined by the reciprocal of

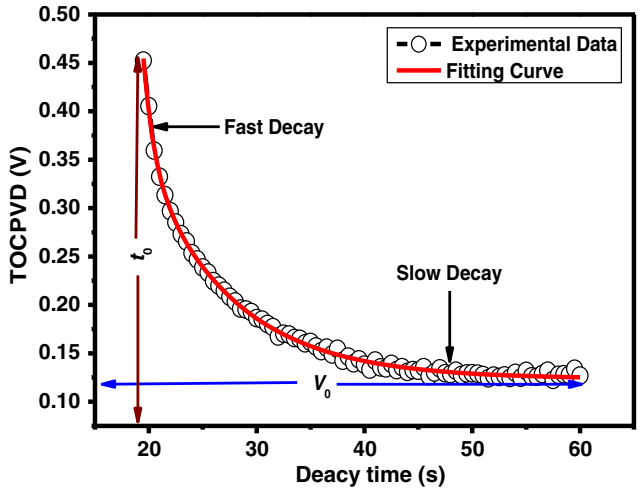

Fig. 9 TOCPVD of DSSCs device based 0.32-mM of EY dye and the red line is the double exponential decay fitted curve.

the derivative of the TOCPVD curve normalized by the thermal voltage ($V_T = K_B T/q$), where K_B is Boltzmann constant, T is the absolute temperature, q is the elementary charge, using the following equation:[41]

$$\tau_n = -V_T \left(\frac{dV_{oc}}{dt}\right)^{-1}. \tag{2}$$

Now, the differentiation reciprocal of Eq. (1) is

$$\left(\frac{dV_{OC}}{dt}\right)^{-1} = \left\{-\left[\frac{V_1}{\tau_1} e^{-(t-t_1)/\tau_1} + \frac{V_2}{\tau_2} e^{-(t-t_2)/\tau_2}\right]\right\}^{-1}. \tag{3}$$

When Eq. (3) substitutes into Eq. (2), it becomes

$$\tau_n = V_T \left\{\left[\frac{V_1}{\tau_1} e^{-(t-t_1)/\tau_1} + \frac{V_2}{\tau_2} e^{-(t-t_2)/\tau_2}\right]\right\}^{-1}. \tag{4}$$

Since the backtransition is usually taken as the pseudofirst-order rate constant, which is related to τ_n as

$$k_{rec} = \frac{1}{\tau_n}. \tag{5}$$

Substitute Eq. (4) into Eq. (5), which becomes

$$k_{rec} = \left[\frac{V_1}{\tau_1} e^{-(t-t_1)/\tau_1} + \frac{V_2}{\tau_2} e^{-(t-t_2)/\tau_2}\right][V_T]^{-1}. \tag{6}$$

Depending on Eq. (1), the fitting parameters for the DSSCs devices that were sensitized with 0.32 mM of EB and EY dyes are tabulated in Table 2. It is notable that the sensitized device with EB dye has a longer lifetime than EY dye. Meanwhile, the recombination rate of the sensitized device with EB dye is slower than that sensitized with EY dye. The results revealed that the τ_n in the ZnO NPs (0.32-mM EB dye)-based DSSC was longer than that in the 0.32-mM EY dye, demonstrating that the latter possessed a higher surface trap density,[42] which might result from the larger surface area. The higher recombination rate and shorter electron lifetime within ZnO NPs photoanode were the reason why the FF of corresponding DSSCs decreased.

As the impedance spectroscopy is not available at our lab to check the electron transport kinetic reaction in the cell, the TOCPVD was investigated more to get deeper insight into the recombination mechanism. TOCPVD proves to be an excellent tool, although the recombination of the photoinjected electrons with the oxidized dye cannot be measured by TOCPVD, as being a dark measurement. When abruptly stopping the irradiation, the TOCPVD yields the approximated lifetime of photoinjected electrons. Under this dark condition, the electron transport resistance within the photoanodes does not influence the TOCPVD measurement since there is no current cycling through the DSSCs. The accumulated electrons in the conduction band and the localized states recombine with the oxidized species and, consequently, the V_{oc} decays due to the shift of the ZnO Fermi level. The dependence of the τ_n on the V_{oc} qualitatively indicates the nature of the electron-trapping mechanism by surface traps and bulk traps that are localized

Table 2 The parameters of the TOCPVD.

			Fast decay		Slow decay			
Dye 0.32 mM	V_0 (V)	t_0 (s)	V_1 (V)	τ_1 (s)	V_2 (V)	τ_2 (s)	τ_n (s)	k_{rev} (s^{-1})
EB	0.1099	12.3573	0.1403	1.1064	0.1329	9.3401	10.4465	0.0957
EY	0.1237	19.4854	0.1067	0.9798	0.2263	8.1563	9.1361	0.1094

electronic states within the bandgap.[6] Surface traps are defined as localized states with shallow traps, allowing charge transfer not only to conduction band states but also to acceptor species such as the oxidized dye (photosensitizer) or acceptor species in the electrolyte.[7] Surface traps stem from superficial amorphous states and can be correlated with the defect characteristic of zinc interstitial.[6] Meanwhile, bulk traps consist of localized states acting as deep charge trapping states allowing charge transfer merely with conduction band states. On the other hand, bulk traps, which restrain the recombination reaction and prolong the lifetime of the trapped electron, can be found at grain boundaries and amorphous states, and can be associated with the deep level of defect states originating from oxygen vacancies.[6] However, this helps in the interpretation of results in the present study and the trend in lifetime decay. The monoexponential function unfortunately did not fit the experimental obtained data for the cell sensitized with EY dye. However, double exponential function fitted the data very well. To confirm the double exponential, a comparison test was also performed using EB sensitizer, which gave the same behavior. Electron lifetime was proposed to quantify the extent of electron recombination with the redox electrolyte and has been proven effective. The response time in the low voltage region depends on the surface trap density in the ZnO NPs photoelectrode, which influences an electron recombination with oxidized dyes, and redox species in the electrolyte. As indicated in Table 2, the estimated lifetimes for EY and EB showed different values. Chao-Po et al.[43] and Wu et al.[44] reported different response times for different dyes with the same electrode. This was referred to as the difference in the surface trap density results from the adsorption of the dye on the ZnO NPs surface.

4 Conclusion

ZnO NPs photoanode were successfully synthesized and mediated by the hydrothermal method. XRD results indicated that a hexagonal wurtzite structure was formed. The HR-TEM micrograph showed that semispherical particles (10 and 40 nm) for ZnO NPs were well crystallized with an intermediate or poor agglomeration. The average ZnO NPs size was confirmed by XRD and HR-TEM inspections. The calculated bandgap of the ZnO NPs was found to be 3.70 ± 0.01 eV, which indicated that a blueshift occurred. The PLES of ZnO NPs were examined and decomposed into two regions: NUV and visible (violet-blue, blue-green, and orange-red). The 0.32-mM EY dye-sensitized cells presented the best DSSCs performance among others. The results showed an enhancement of both the J_{sc} and the V_{oc} for the EY dye-sensitized cells compared to the EB dye-sensitized cells, which is attributed to the higher dye loading of the EY dye on the surface of the ZnO NPs.

Acknowledgments

This research activity carried out between Gaza and Cairo-Egypt was financially supported by Qatar Charity IBHATH Project grant funded by the Gulf Cooperation Council for the Reconstruction of Gaza through the Islamic Development Bank.

References

1. G. W. Crabtree and N. S. Lewis, "Solar energy conversion," *Phys. Today* **60**(3), 37–42 (2007).
2. A. Goetzberger and C. Hebling, "Photovoltaic materials, past, present, future," *Sol. Energy Mater. Sol. Cells* **62**(1–2), 1–19 (2000).
3. R. A. Kerr, "How urgent is climate change," *Science* **318**(5854), 1230–1231 (2007).
4. R. D. McConnell, "Assessment of the dye-sensitized solar cell," *Renewable Sustainable Energy Rev.* **6**, 271–293 (2002).
5. B. O'Regan and M. Gratzel, "A low-cost, high-efficiency solar cell based on dye-sensitized colloidal TiO_2 films," *Nature* **353**, 737–740 (1991).
6. R. A. Wahyuono et al., "Effect of annealing on the sub-bandgap, defects and trapping states of ZnO nanostructures," *Chem. Phys.* **483–484**, 112–121 (2017).

7. R. A. Wahyuono et al., "ZnO nanostructures-based dye-sensitized solar cells using the $TEMPO^+$/TEMPO redox mediator and ruthenium(II) photosensitizer with 1, 2, 3-triazole-derived ligands," *ChemPlusChem* **81**(12), 1281–1291 (2016).
8. R. A. Wahyuono et al., "ZnO nanoflowers-based photoanodes: aqueous chemical synthesis, microstructure and optical properties," *Open Chem.* **14**, 158–169 (2016).
9. P. Baviskar, A. Ennaoui, and B. Sankapal, "Influence of processing parameters on chemically grown ZnO films with low cost Eosin-Y dye towards efficient dye sensitized solar cell," *Sol. Energy* **105**, 445–454 (2014).
10. M. Graetzel, "Dye-sensitized solar cells," *J. Photochem. Photobiol. C Photochem. Rev.* **4**, 145–153 (2003).
11. J. Bandara, U. W. Pradeep, and R. G. S. J. Bandara, "The role of n-p junction electrodes in minimizing the charge recombination and enhancement of photocurrent and photovoltage in dye sensitized solar cells," *J. Photochem. Photobiol. A Chem.* **170**(3), 273–278 (2005).
12. D. Kuang et al., "High-efficiency and stable mesoscopic dye-sensitized solar cells based on a high molar extinction coefficient ruthenium sensitizer and nonvolatile electrolyte," *Adv. Mater.* **19**(8), 1133–1137 (2007).
13. Q. Zhang and G. Cao, "Nanostructured photoelectrodes for dye-sensitized solar cells," *Nano Today* **6**(1), 91–109 (2011).
14. M. K. Nazeeruddin et al., "Conversion of light to electricity by cis-X2bis(2, 2′-bipyridyl-4, 4′-dicarboxylate)ruthenium(II) charge-transfer sensitizers (X = Cl-, Br-, I-, CN-, and SCN-) on nanocrystalline titanium dioxide electrodes," *J. Am. Chem. Soc.* **115**(14), 6382–6390 (1993).
15. M. K. Nazeeruddin et al., "Acid–base equilibria of (2, 2'-bipyridyl-4, 4'-dicarboxylic acid) ruthenium(ii) complexes and the effect of protonation on charge-transfer sensitization of nanocrystalline titania," *Inorg. Chem.* **38**(26), 6298–6305 (1999).
16. A. Islam et al., "Sensitization of nanocrystalline TiO_2 film by ruthenium(II) diimine dithiolate complexes," *J. Photochem. Photobiol. A Chem.* **145**(1–2), 135–141 (2001).
17. H. Gerischer et al., "Sensitization of charge injection into semiconductors with large band gap," *Electrochim. Acta* **13**(6), 1509–1515 (1968).
18. T. Watanabe et al., "pH-dependence of spectral sensitization at semiconductor electrodes," *Bull. Chem. Soc. Jpn.* **49**(1), 8–11 (1976).
19. H. Tsubomura et al., "Dye sensitised zinc oxide: aqueous electrolyte: platinum photocell," *Nature* **261**, 402–403 (1976).
20. F. Labat et al., "First principles modeling of eosin-loaded ZnO films: a step toward the understanding of dye-sensitized solar cell performances," *J. Am. Chem. Soc.* **131**, 14290 (2009).
21. A. Zaban et al., "Determination of the electron lifetime in nanocrystalline dye solar cells by photovoltage decay measurements," *ChemPhysChem* **4**, 859–864 (2003).
22. V. Kumar et al., "Origin of the red emission in zinc oxide nanophosphors," *Mater. Lett.* **101**, 57–60 (2013).
23. M. Ghosh et al., "Shape transition in ZnO nanostructures and its effect on blue-green photoluminescence," *Nanotechnology* **19**(44), 445704 (2008).
24. S. R. Brintha et al., "Synthesis and characterization of ZnO nanoparticles via aqueous solution, sol-gel and hydrothermal methods," *IOSR J. Appl. Chem.* **8**(11), 66–72 (2015).
25. S. K. K. Shaat et al., "Investigation of luminescent properties of $Ca_{0.3}Sr_{0.7}Al_2O_4:Tb^{3+}$, Eu^{3+} excited using different excitation sources," *J. Electron. Spectrosc. Relat. Phenom.* **197**, 72–79 (2014).
26. L. Irimpan, V. P. N. Nampoori, and P. Radhakrishnan, "Size dependent fluorescence spectroscopy of nanocolloids of ZnO," *J. Appl. Phys.* **102**, 063524 (2007).
27. C. E. Kim et al., "Effect of carrier concentration on optical bandgap shift in ZnO:Ga thin films," *Thin Solid Films* **518**(22), 6304–6307 (2010).
28. P. M. Aneesh, K. A. Vanaja, and M. K. Jayaraj, "Synthesis of ZnO nanoparticles by hydrothermal method," *Proc. SPIE* **6639**, 66390J (2007).
29. J.-H. Lin et al., "Photoluminescence mechanisms of metallic Zn nanospheres, semiconducting ZnO nanoballoons, and metal-semiconductor Zn/ZnO nanospheres," *Sci. Rep.* **4**(6967), 1–8 (2014).

30. N. Shakti et al., "Processing temperature dependent morphological and optical properties of ZnO nanorods," *Mater. Sci. Semicond. Process.* **20**, 55–60 (2014).
31. K. Lim et al., "Temperature-driven structural and morphological evolution of zinc oxide nano-coalesced microstructures and its defect-related photoluminescence properties," *Materials* **9**(4), 300–315 (2016).
32. T. T. John et al., "Effect of $[OH^-]$ linkages on luminescent properties of ZnO nanoparticles," *J. Phys. Chem. C* **115**(37), 18070 (2011).
33. S. Al-Hilli et al., "The pH response and sensing mechanism of n-type ZnO/electrolyte interfaces," *Sensors* **9**(9), 7445–7480 (2009).
34. Y. H. Yang et al., "Physical mechanism of blue-shift of UV luminescence of a single pencil-like ZnO nanowire," *Nano Lett.* **7**(12), 3879–3883 (2007).
35. T. P. Chou, Q. Zhang, and G. Cao, "Effects of dye loading conditions on the energy conversion efficiency of ZnO and TiO_2 dye-sensitized solar cells," *J. Phys. Chem. C* **111**, 18804 (2007).
36. V. Thavasi et al., "Controlled electron injection and transport at materials interfaces in dye sensitized solar cells," *Mater. Sci. Eng. R* **63**, 81–99 (2009).
37. A. A. Waheed et al., "Mechanism of dye binding in the protein assay using Eosin dyes," *Anal. Biochem.* **287**(1), 73–79 (2000).
38. C. J. Brabec et al., "Origin of the open circuit voltage of plastic solar cells," *Adv. Funct. Mater.* **11**(5), 374–380 (2001).
39. S. Jang et al., "High molar extinction coefficient ruthenium sensitizers for thin film dye-sensitized solar cells," *J. Phys. Chem. C* **113**(5), 1998–2003 (2009).
40. S. Zhu et al., "Hydrothermal synthesis of oriented ZnO nanorod–nanosheets hierarchical architecture on zinc foil as flexible photoanodes for dye-sensitized solar cells," *Ceram. Int.* **40**(8), 11663 (2014).
41. Z. Zhang, "École polytechnique fédérale de lausanne," PhD Thesis, Switzerland (2008).
42. C. Xu et al., "Ordered TiO_2 nanotube arrays on transparent conductive oxide for dye-sensitized solar cells," *Chem. Mater.* **22**(1), 143–148 (2010).
43. C. Hsu et al., "EIS analysis on low temperature fabrication of TiO_2 porous films for dye-sensitized solar cells," *Electrochim. Acta* **53**, 7514–7522 (2008).
44. J. Wu et al., "Effects of dye adsorption on the electron transport properties in ZnO-nanowire dye-sensitized solar cells," *Appl. Phys. Lett.* **90**, 213109 (2007).

Samy Shaat is an assistant professor in the Physics Department at the Islamic University, Palestine. He occupied different administrative positions since 1998. He was as a postdoc at the University of the Free State (UFS), South Africa, after he got his PhD from UFS. He registered some distinguished data as a patent and was awarded several prestigious scholarship and prizes. He published his data in several prestigious journals and presented his data in international conferences. His areas of interests are applied science, technical, vocational, training, etc. His area of research is in materials science (synthesis and characterization) and engineering for nanotechnology applications such as energy production and storage.

Hamdia Zayed obtained her PhD in solid-state physics from Bucharest State University, Romania. She was the dean of Women's College for Art, Science, and Education, Ain Shams University, Cairo, Egypt. Her research interest has been focused on nanomaterials synthesis and electrical and optical properties of nanomaterials.

Hussam Musleh is a PhD student in the Physics Department, Ain Shams University, Cairo. His areas of interests are nanomaterials synthesis and characterization and fabrication of nanomaterials for solar cell specially dye sensitized solar cells.

Nabil Shurrab received his BSc degree from Birzeit University—West Bank, his MSc degree from link program Al-Azhar University—Manchester University, England, and his PhD from Cairo University. He is an assistant professor of organic chemistry at Al-Azhar University—Gaza. He is currently the chairman in the Chemistry Department at AUG. The research interest is focusing on the synthetic organic chemistry, specialized on the investigation of new methods

for the synthesis of versatile and hitherto unreported heterocyclic compounds of expected biological activity.

Ahmed Issa received his bachelor of mechatronics from International Islamic University—Malaysia, in 2001 and his doctorate of mechanical and manufacturing engineering from Dublin City University—Ireland, in 2007. He is currently an assistant professor of mechatronics and the head of the Engineering Department, Faculty of EIT, Al-Azhar University—Gaza, Palestine. His research interests in measurements, instrumentation, control systems, automation, and RP technologies, as well as laser processing of materials and thermal mathematical modeling.

Jihad Asad is a young assistance researcher working at the materials science and engineering research group supervision by Professor AlDahoudi.

Naji Al Dahoudi is a professor of physics and materials sciences at the Physics Department, Al-Azhar University—Gaza, Palestine. He got the PhD from the Leibniz Institute of New Materials, Saarbruecken/Germany. More than 40 of his research work have been presented and published at several international congresses scientific journals. His research interest is concentrated on synthesis of nanostructured functional materials, such as TCO, gas sensors and currently has conducted a new trend of research on renewable energy using nanostructured materials for dye sensitized and perovskite solar cells.